

# van der Waals Modes of Solute/Solvent Clusters: Benzene–Methane, –Deuteriomethane, and –Carbon Tetrafluoride

J. A. Menapace and E. R. Bernstein\*

Department of Chemistry, Condensed Matter Sciences Laboratory, Colorado State University, Fort Collins, Colorado 80523 (Received: October 20, 1986)

Clusters of benzene( $\text{CD}_4$ )<sub>1</sub> and  $-(\text{CF}_4)$ <sub>1</sub> are created in a supersonic molecular jet and are studied by two-color time-of-flight mass spectroscopy. The clusters'  $S_1 \leftarrow S_0$  intermolecular vibronic structures are characterized by calculational modeling of the clusters' intermolecular motion. The calculations include (1) an intermolecular normal-coordinate analysis (NCA) which treats all six van der Waals modes under a harmonic oscillator assumption and (2) a three-dimensional hindered rigid-rotor analysis (3D-HRRA) which treats the intermolecular torsional motion. Agreement between calculation and experiment is excellent for binding energy, symmetries, and van der Waals mode energies. The cluster spectra and calculated intermolecular modes are compared to those of benzene( $\text{CH}_4$ )<sub>1</sub> reported previously. A major conclusion of this work is that the clusters behave rigidly with regard to internal rotation of the cluster subunits and that the clusters possess unique equilibrium geometries. The internal torsional motion is oscillatory and is constrained by an orientationally dependent intermolecular potential whose barrier height is of the order of the cluster binding energy.

## Introduction

van der Waals (vdW) complexes of aromatic molecules with hydrocarbon solvents form a class of supramolecular systems whose intermolecular bonding has several interesting features. First, the intermolecular interaction is small and is dominated by long-range dispersive attractions and short-range exchange repulsions. These two features allow the interaction to be modeled by an intermolecular potential of known functional form. For example, the interaction can be modeled by additive atom–atom potentials set in a Lennard-Jones or an exponential-six format.<sup>1</sup> Second, the interaction potential surface only changes slightly, if at all, upon electronic excitation of the cluster chromophore. Thus, small spectral shifts of the chromophore electronic transition and weak intensity intermolecular vdW mode vibronic transitions are observed.<sup>2,3</sup> Third, the interaction results in the formation of specific minimum-energy cluster configurations. These geometries are interesting since they give insight into the nucleation processes and solvation geometry occurring in both gas- and condensed-phase systems.<sup>1</sup> Fourth, the small binding energy of the complex and the low-frequency vdW vibrational modes are important since they play an essential role in intramolecular vibrational redistribution (IVR) and vibrational predissociation (VP) cluster dynamic energy-transfer processes.<sup>4</sup> And fifth, cluster structure, binding energy, vdW modes, and dynamics (IVR and VP) are essentially dependent on the actual cluster structure and the intricacies of the intermolecular interaction.<sup>3,5</sup>

In this paper, we report the spectroscopic results of the benzene–deuteriated methane ( $\text{ben}(\text{CD}_4)_1$ ) and benzene–carbon tetrafluoride ( $\text{ben}(\text{CF}_4)_1$ ) clusters together with calculated modeling of selected cluster characteristics. The spectroscopic results include the  $\pi^* \leftarrow \pi$  vibronic spectra of the clusters in their respective benzene constituent  $6_0^1$  regions.

The calculated results include the geometry, the binding energy, and the full eigenvalue/eigenvector intermolecular vibrational structure for the electronic ground state of each cluster. The intermolecular ground-state vibrational structure is modeled by two methods: (1) an intermolecular normal-coordinate analysis (NCA) which determines all six intermolecular vdW mode fundamentals under a harmonic oscillator assumption<sup>3</sup> and (2) a

three-dimensional hindered rigid-rotor analysis (3D-HRRA) for which an anisotropic perturbation field is applied to the cluster solvents considered to be rigid internal rotors in the resulting potential well. The intermolecular torsional mode structure is thereby obtained under a hindered rigid-rotor approximation.

The calculated ground-state vibrational structure for each cluster is compared to its experimental vibronic spectrum and to the structure observed and calculated for the benzene–methane ( $\text{ben}(\text{CH}_4)_1$ ) cluster.<sup>1,3</sup> Within this framework, vibronic selection rules which govern the clusters'  $S_1 \leftarrow S_0$  transitions are discussed along with the ramifications of Herzberg–Teller (H–T) coupling for the observation of “forbidden” vibronic transitions.

The motivation for studying these systems concerns the elucidation of the vdW torsional structure. Two limiting cases can be proposed in regard to the torsional structure of  $\text{ben}(\text{CH}_4)_1$ ,  $\text{ben}(\text{CD}_4)_1$ , and  $\text{ben}(\text{CF}_4)_1$ . In one case, the clusters possess free internal rotation between the cluster solute and solvent. The cluster solvent ( $\text{CH}_4$ ,  $\text{CD}_4$ , or  $\text{CF}_4$ ) rotates freely in three dimensions against the benzene framework, and the system is considered nonrigid. In the other case, the clusters possess torsional oscillations for which the cluster solvent librates against the benzene frame with a residence time long enough to give rise to “vibration-like” motion in a rigid-molecule regime.

Elucidation of the vdW torsions is of particular interest in these systems since the aforementioned limiting cases pose questions regarding the actual physics governing the torsional structure: (1) Do the clusters possess free internal rotation between the cluster solute and solvent or do they possess torsional oscillations for which the lowest eigenstates behave more or less harmonically? (2) In either case, what is the dependence of the intermolecular potential upon the relative orientation of the cluster constituents?

## Experimental Procedures

The apparatus and techniques employed in this study are largely the same as those previously reported.<sup>1,3</sup> The  $\text{ben}(\text{CD}_4)_1$  and  $\text{ben}(\text{CF}_4)_1$  spectra are recorded by using a pulsed supersonic molecular jet expansion in combination with two-color time-of-flight mass spectroscopy (2-color TOFMS). Two  $\text{Nd}^{3+}$ :YAG pumped dye lasers are used to probe the cluster spectra. An LDS 698 dye laser whose output is frequency-doubled and mixed with the  $\text{Nd}^{3+}$ :YAG 1.064- $\mu\text{m}$  fundamental is used to probe the clusters'  $S_1 \leftarrow S_0$  transition in the isolated benzene  $6_0^1$  region ( ${}^1\text{B}_{2u} \leftarrow {}^1\text{A}_{1g}$ ;  $\pi^* \leftarrow \pi$ ). Subsequent ionization of the clusters is accomplished with a R590 dye laser whose output is frequency-doubled and mixed with the  $\text{Nd}^{3+}$ :YAG 1.064- $\mu\text{m}$  fundamental. The ionization laser output is set at 45 112  $\text{cm}^{-1}$ . A 5% mixture of deuteriated methane or carbon tetrafluoride in helium is placed in line with liquid benzene in a trap at room temperature. The three-component mixture is expanded with a pulsed molecular

(1) Schauer, M.; Bernstein, E. R. *J. Chem. Phys.* **1985**, *82*, 726. Schauer, M.; Law, K. S.; Bernstein, E. R. *J. Chem. Phys.* **1985**, *82*, 736. Wanna, J.; Bernstein, E. R. *J. Chem. Phys.* **1986**, *84*, 927.

(2) Stephenson, T. A.; Rice, S. A. *J. Chem. Phys.* **1984**, *81*, 1083.

(3) Menapace, J. A.; Bernstein, E. R. *J. Phys. Chem.*, in press, and references therein.

(4) Beswick, J. A.; Jortner, J. *J. Chem. Phys.* **1981**, *74*, 6725, and references therein. Kelley, D. F.; Bernstein, E. R., to be submitted for publication in *J. Phys. Chem.*

(5) Kelley, D. F.; Bernstein, E. R. *J. Phys. Chem.* **1986**, *90*, 5164.

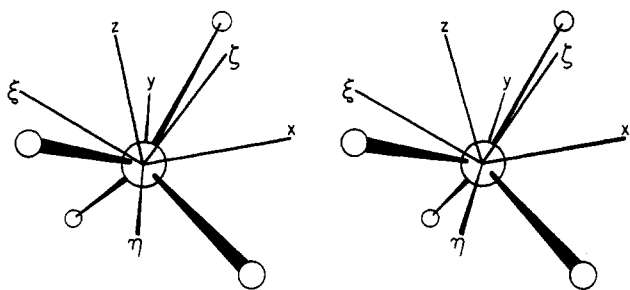


**Figure 1.** Stereoscopic projection of solvent tetrahedron showing relative orientation of the molecule-fixed ( $x, y, z$ ) and space-fixed ( $\xi, \eta, \zeta$ ) coordinate systems used in the 3D-HRRA. The ( $x, y, z$ ) coordinate system is located at  $\theta = 45^\circ$ ,  $\phi = 0^\circ$ , and  $\chi = 180^\circ$  from the ( $\xi, \eta, \zeta$ ) coordinate system.

jet nozzle having a 500- $\mu\text{m}$  orifice while maintaining 100 psig backing pressure. Apparatus chamber pressure is maintained at or below  $5 \times 10^{-6}$  Torr during the experiments.

### Theoretical Considerations

The NCAs are conducted by using the same methods as described in our previous publication on vdW cluster vibronic structure.<sup>3</sup> For  $\text{ben}(\text{CD}_4)_1$ , the calculated cluster ground-state geometry, force field, and binding energy are taken as those of  $\text{ben}(\text{CH}_4)_1$ . Only the masses are changed for the deuterium/hydrogen substitutions in the NCA. For  $\text{ben}(\text{CF}_4)_1$ , the cluster ground-state geometry and binding energy are calculated via intermolecular energy minimization employing the methods previously described.<sup>1,3</sup> The NCA is conducted by using the modeled geometry and its corresponding force field. The potential parameters for the C-F ( $A_{\text{CF}} = 6.08 \times 10^7 \text{ cm}^{-1}/\text{\AA}^{12}$ ;  $C_{\text{CF}} = 1.13 \times 10^5 \text{ cm}^{-1}/\text{\AA}^6$ ) and H-F ( $A_{\text{HF}} = 7.77 \times 10^6 \text{ cm}^{-1}/\text{\AA}$ ;  $C_{\text{HF}} = 3.12 \times 10^4 \text{ cm}^{-1}/\text{\AA}$ ) atom-atom interactions are determined from parameters and methods described elsewhere.<sup>6</sup>

The 3D-HRRA centers upon analyzing the effects of the intermolecular potential on the cluster solvent rotational degrees of freedom. In the absence of a perturbing field from the cluster solute, the cluster solvent rotates freely in three dimensions against a fixed cluster solute framework. Application of a specified perturbation field results in the eventual restriction of this free rotation to torsional oscillation as the perturbation field magnitude is increased; that is, rotation ceases and vibrational oscillatory motion begins as the residence times of the solvent in the torsional potential well becomes longer.

In the 3D-HRRA, both clusters constituents are assumed internally rigid, their respective internal geometries remaining constant and at "equilibrium". The cluster solvents are taken as the rotating portions of the clusters since their zero-field rotational constants are orders of magnitude greater than those of the cluster solute. The hindered solvent rotations are presupposed to contribute to the spectral features observed along with the intermolecular bending and stretching modes.

The 3D-HRRA involves setting up a molecule-fixed coordinate system ( $x, y, z$ ) and a space-fixed coordinate system ( $\xi, \eta, \zeta$ ) on the cluster solvent, as shown in Figure 1. Both systems have their origins at the nuclear center-of-mass of the cluster solvent. The molecule-fixed coordinate system is chosen such that its principle axes lie along the  $C_2$  rotational axes of the solvent tetrahedron ( $T_d$  point group symmetry). The space-fixed coordinate system is chosen to be at the Euler angles  $\theta = 45^\circ$ ,  $\phi = 0^\circ$ , and  $\chi = 180^\circ$  with respect to the molecule-fixed coordinate system. The relative orientation of these two systems is chosen so that the orientational dependence of the perturbation field can be expressed as a simple function of the curvilinear coordinates  $\theta$ ,  $\phi$ , and  $\chi$ .

An analytical expression for the potential governing the torsional motion can be derived by analyzing the solvent rotations in each

of the rotational coordinates. Since a solvent rotation is periodic over  $360^\circ$ , the potential can be expressed by an even function Fourier series written as<sup>7</sup>

$$V(q) = V_0/2 + \sum_{p=1}^{\infty} A_p \cos(pq) \quad (1)$$

with  $q$  a function of the rotational coordinates and  $V_0$  taken as the barrier height to internal rotation. The function  $q$  is determined by the potential dimensionality and the number of minima in the potential along each of the rotational coordinates. The first cosine term in the series describes the major form of the potential, and the rest of the terms in the series "fine tune" the potential shape. Since the coefficients  $A_p$  in these terms are assumed to be small, the series can be truncated at its first cosine term without sacrificing the general potential shape. Doing this yields the mathematically convenient potential form

$$V(q) = \frac{V_0}{2}(1 - \cos(q)) \quad (2)$$

The symmetry of the cluster of solvents can be employed to determine the dimensionality of and the number of minima in the potential and, hence, the function  $q$ . Rotating the cluster solvents against the benzene frame by  $90^\circ$  in  $\theta$  or  $\chi$ ,  $270^\circ$  in  $\chi$ , or  $180^\circ$  in the  $\phi$  coordinate results in equivalent maxima. Equivalent minima occur at  $0^\circ$  rotation in  $\theta$ ,  $\phi$ , and  $\chi$  and at  $180^\circ$  rotation in  $\theta$  and  $\chi$ . The maxima have the same energy  $V_0$  relative to the equivalent minima in all three rotational coordinates. Generalizing these relative displacements to all coordinate values, one finds that the potential magnitude depends upon the relative displacements of all three rotational coordinates as

$$q = 2\theta + 2\chi + \phi \quad (3)$$

Inserting eq 3 into eq 2 yields the three-dimensional potential function used in the calculations

$$V(\theta, \phi, \chi) = \frac{V_0}{2}[1 - \cos(2\theta + 2\chi + \phi)] \quad (4)$$

in which  $V_0$  is the barrier height to internal rotation. The rotational wave functions chosen as the basis set for the calculation are the rigid-rotor symmetric top wave functions which depend on the curvilinear coordinates and on the quantum numbers  $J$ ,  $k$ , and  $m$ . Under zero-field conditions, these wave functions are solutions to the spherical top Schrödinger equation<sup>8</sup>

$$\frac{-B}{\hbar^2} \hat{J}^2 |jkm\rangle = E_{\text{rot}}^j |jkm\rangle \quad (5)$$

with eigenvalues corresponding to those of the spherical top cluster solvent. Upon application of the perturbation field, the eigenvalues are obtained via diagonalization of the energy matrix possessing elements of the form

$$\left\langle J'k'M \left| \frac{-B}{\hbar^2} \hat{J}^2 + V(\theta, \phi, \chi) \right| J''k''m'' \right\rangle \quad (6)$$

using eq 1 for  $V(\theta, \phi, \chi)$  with  $V_0$  as an adjustable parameter. In the calculations performed, the only possible nonzero off-diagonal matrix elements occur with the following restrictions:

$$|J' - J''| \leq 2 \quad (7)$$

$$|k' - k''| = 2 \quad (8)$$

$$|m' - m''| = 1 \quad (9)$$

Diagonal matrix elements contain only the zero-field spherical top energies and a  $V_0/2$  potential term.

(6) Miller, T. M.; Bederson, B. *Adv. At. Mol. Phys.* **1977**, *13*, 1. *Handbook of Chemistry and Physics*, 53rd ed.; CRC Press: Boca Raton, FL, 1973. Nemethy, G.; Pottle, M. S.; Scheraga, H. A. *J. Phys. Chem.* **1983**, *87*, 1883, and references therein.

(7) Crawford Jr., B. L. *J. Chem. Phys.* **1940**, *8*, 273. Pitzer, K. S.; Gwinn, W. D. *J. Chem. Phys.* **1942**, *10*, 428. Herzberg, G. *Molecular Spectra and Molecular Structure: II. Infrared Raman Vibrational Spectra*; McGraw-Hill: New York, 1955.

(8) Bunker, P. R. *Molecular Symmetry and Spectroscopy*; Academic: New York, 1979.

TABLE I: vdW Spectral Features in  $\text{ben}(\text{CD}_4)_1$  and  $\text{ben}(\text{CH}_4)_1$   $6_0^1$  Regions and Calculated Ground-State vdW Modes (Refer to Figure 2)

$\text{ben}(\text{CD}_4)_1$				$\text{ben}(\text{CH}_4)_1^d$			
energy <sup>a</sup>				energy <sup>a</sup>			
obsd	NCA	3D-HRRA <sup>c</sup>	assign <sup>t</sup> <sup>b</sup>	obsd	NCA	3D-HRRA <sup>c</sup>	assign <sup>t</sup> <sup>b</sup>
0 <sup>e</sup>	0	0 (4)	$6_0^1$	0 <sup>f</sup>	0	0 (4)	$6_0^1$
16.1	15 ( $b_{xy}$ )		$6_0^1 b_{xy}^1$	16.1	16 ( $b_{xy}$ )		$6_0^1 b_{xy}^1$
22.5	20 ( $t_z$ )	21 (4)	$6_0^1 t_{z0}^1$	27.3	28 ( $t_z$ )	29 (4)	$6_0^1 t_{z0}^1$
32			$6_0^1 b_{xy}^2$	32.3			$6_0^1 b_{xy}^2$
			$6_0^1 b_{xy}^3$	48.4			$6_0^1 b_{xy}^3$
48.4		47 (4)	$6_0^1 t_{z0}^2$	51.4		54 (2)	$6_0^1 t_{z0}^2$
58.1	64 ( $t_{xy}$ )	68 (8)	$6_0^1 t_{xy0}^1$				
62.7			$6_0^1 b_{xy}^4$	64.6			$6_0^1 b_{xy}^4$
70.5		75 (4)	$6_0^1 t_{z0}^3$	73.5		73 (4)	$6_0^1 t_{z0}^3$
72.9	75 ( $s_z$ )		$6_0^1 s_{z0}^1$		82 ( $s_z$ )		
84		80 (12)	$6_0^1 t_{xy0}^1 t_{z0}^1$		89 ( $t_{xy}$ )	84 (8)	
93.3			$6_0^1 s_{z0}^1 b_{xy}^1$				
97.5			$6_0^1 s_{z0}^1 t_{z0}^1$				
100			$6_0^1 t_{z0}^4$				

<sup>a</sup>Energies are reported in  $\text{cm}^{-1}$  relative to the  $6_0^1$  cluster origins. <sup>b</sup>vdW mode representations as per Figure 2. <sup>c</sup>Values in parentheses represent "structural" degeneracy calculated in 3D-HRRA. <sup>d</sup>From ref 1 and 3. <sup>e</sup>At  $38\,567.4\text{ cm}^{-1}$ . <sup>f</sup>At  $38\,567.6\text{ cm}^{-1}$ .

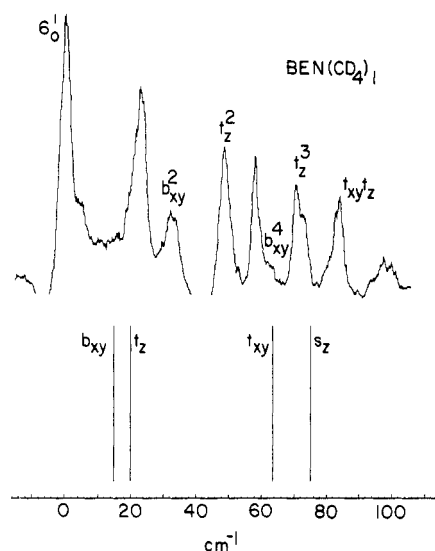


Figure 2. Two-color TOFMS  $S_1 \leftarrow S_0$  spectrum and calculated ground-state vdW modes (NCA) of  $\text{ben}(\text{CD}_4)_1$ . Energy scale is relative to  $\text{ben}(\text{CD}_4)_1$   $6_0^1$  transition ( $38\,567.4\text{ cm}^{-1}$ ). Feature positions and assignments as per Table I and Figure 3.

The resulting matrix is diagonalized for a selected value of  $V_0$  yielding eigenvalues corresponding to the solvent torsional eigenstates at the specified perturbation. The perturbation is varied until a reasonable fit with the experimental spectrum is obtained. The calculations are performed on a Cyber 205 computer using a basis set consisting of 680 wave functions to ensure convergence of the lowest eigenstates at their proper eigenvalues. Only the torsional structures of  $\text{ben}(\text{CH}_4)_1$  and  $\text{ben}(\text{CD}_4)_1$  are calculated since their respective rotational constants are large enough that the coupling of the rotational levels does not require an extremely large basis set to ensure convergence. Matrix elements are determined via numerical integration using a nonadaptive integration routine. The matrix is prediagonalized into a tridiagonal form by using orthogonal similarity transformations<sup>9</sup> and diagonalized by using an implicit QL method.<sup>10</sup> The rotational constants used for methane and deuterated methane are  $5.2$  and  $2.6\text{ cm}^{-1}$ , respectively.

## Results

**$\text{Ben}(\text{CD}_4)_1$ .** Figure 2 and Table I present the  $\text{ben}(\text{CD}_4)_1$  vdW cluster spectrum in the region between  $38\,552.4$  and  $38\,678.6\text{ cm}^{-1}$

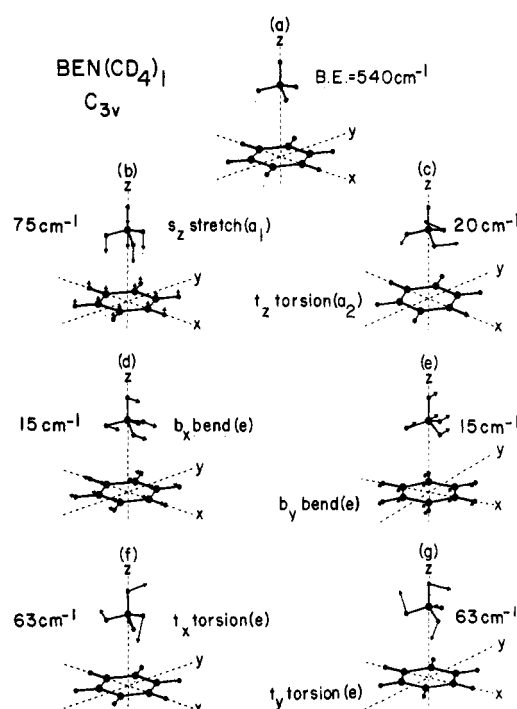


Figure 3. Calculated ground-state minimum-energy configuration (a) and NCA eigenvalue/eigenvector vdW modes (b)–(g) for  $\text{ben}(\text{CD}_4)_1$ . Cluster symmetry is  $C_{3v}$  with an equilibrium intermolecular distance of  $3.47\text{ \AA}$ . Eigenvectors are normalized and displayed at  $2\times$  magnification ( $2\text{-\AA}$  total displacement).

obtained by 2-color TOFMS. The cluster  $6_0^1$  transition is "red-shifted" by  $41.2\text{ cm}^{-1}$  with respect to the benzene  $6_0^1$ . The bathochromic shift is comparable to that of  $\text{ben}(\text{CH}_4)_1$  ( $41\text{ cm}^{-1}$ ), indicating that the binding energy difference between  $S_1$  and  $S_0$  for  $\text{ben}(\text{CD}_4)_1$  is nearly identical with that of  $\text{ben}(\text{CH}_4)_1$ . Ten pronounced intermolecular vibronic features are observed to the "blue" of the cluster  $6_0^1$ . As in the case of the  $\text{ben}(\text{CH}_4)_1$  cluster, no features are observed in the symmetry-forbidden benzene  $0_0^0$  region. Thus, the cluster geometry must possess at least a threefold axis of symmetry.

The calculated  $\text{ben}(\text{CD}_4)_1$  geometry (Figure 3) is assumed to be the same as that calculated for  $\text{ben}(\text{CH}_4)_1$ . The geometry possesses  $C_{3v}$  point group symmetry. In this geometry, the  $\text{CD}_4$  center-of-mass lies  $3.47\text{ \AA}$  above the benzene molecular plane along the threefold rotational axis. The ground-state binding energy in this configuration is calculated at  $540\text{ cm}^{-1}$ . Using the cluster "red shift" of  $41.2\text{ cm}^{-1}$ , we calculated the excited-state binding energy to be  $581\text{ cm}^{-1}$ .

(9) Martin, R. S.; Reinsch, C.; Wilkinson, J. H. *Num. Math.* **1968**, *11*, 181.

(10) Martin, R. S.; Wilkinson, J. H. *Num. Math.* **1968**, *12*, 377. Dubrille, A. *Num. Math.* **1970**, *15*, 450.

**TABLE II: vdW Spectral Features in  $\text{ben}(\text{CF}_4)_1$   $6_0^1$  Region and Calculated Ground-State vdW Modes (Refer to Figure 4)**

obsd	energy <sup>a</sup>		assign <sup>b</sup>
	obsd	NCA	
0 <sup>c</sup>	0		$6_0^1$
15.7	11 ( $b_{xy}$ )		$6_0^1 b_{xy}^1$
17.4	13 ( $t_z$ )		$6_0^1 t_{z0}$
32.3			$6_0^1 b_{xy}^2$
35.4			$6_0^1 t_{z0}^2$
39.5	36 ( $t_{xy}$ )		$6_0^1 t_{xy}^1$
	69 ( $s_z$ )		

<sup>a</sup>Energies are reported in  $\text{cm}^{-1}$  relative to the  $6_0^1$  cluster origin.  
<sup>b</sup>vdW mode representations as per Figure 4. <sup>c</sup>at  $38\,614.7\text{ cm}^{-1}$ .

The NCA reveals six vdW vibrations (Figure 3 and Table I), two being twofold degenerate. The ground-state vibrational energies are  $75\text{ cm}^{-1}$  for the vdW stretch  $s_z(a_1)$ ,  $15\text{ cm}^{-1}$  for the bends  $b_{xy}(e)$ , and  $20\text{ cm}^{-1}$  ( $t_z(a_2)$ ) and  $64\text{ cm}^{-1}$  ( $t_{xy}(e)$ ) for the vdW torsions. The eigenvector normal modes (Figure 3) transform in an identical fashion to those calculated for  $\text{ben}(\text{CH}_4)_1$ . The vdW stretching mode transforms as the translation of the cluster constituents away from one another along the  $z$  (threefold) axis. The vdW bends transform as some combination of cluster constituent translations in opposite directions perpendicular to the threefold axis in the  $xy$  plane. One vdW torsion transforms as a rotation of the cluster constituents about the threefold axis in opposite directions. The remaining two vdW torsions transform as rotations about orthogonal axes perpendicular to the threefold axis.

The 3D-HRRA results are also included in Table I for the lowest eigenstates in the torsional manifold. The torsional mode structure is calculated for  $V_0 = 300\text{ cm}^{-1}$  and  $B = 2.6\text{ cm}^{-1}$ . This perturbation results in a reasonable fit for the torsional features observed experimentally. The torsional "zero-point energy" is  $75\text{ cm}^{-1}$ . Two distinct torsional manifolds result from the calculations: one manifold has eigenvalues grouped quartically (nearly fourfold degenerate located at approximately 21, 46, and  $75\text{ cm}^{-1}$  above the zero-point energy), and the other manifold has eigenvalues grouped octally (nearly eightfold degenerate located at approximately  $68\text{ cm}^{-1}$  above the torsional zero-point energy).

For comparison, the observed vibronic features for  $\text{ben}(\text{CH}_4)_1$  are reproduced in Table I along with the results of the NCA and the 3D-HRRA. The NCA results for  $\text{ben}(\text{CH}_4)_1$  are those reported previously.<sup>3</sup> The 3D-HRRA torsional structure is calculated for  $V_0 = 300\text{ cm}^{-1}$  and  $B = 5.2\text{ cm}^{-1}$ . This perturbation is chosen since it is assumed that the barrier to internal rotation is nearly identical in the two systems as they only differ by isotopic substitution and have the same electronic structure. Additionally, using the same potential barrier of electronic origin for both  $\text{CH}_4$  and  $\text{CD}_4$  clusters provides a check on the validity of the model in predicting the torsional mode structure of the clusters. For  $\text{ben}(\text{CH}_4)_1$  the torsional "zero-point energy" is  $96\text{ cm}^{-1}$ . As in the case of the  $\text{ben}(\text{CD}_4)_1$  calculations, two distinct torsional manifolds result: one manifold with eigenvalues grouped quartically at about 29, 54, and  $73\text{ cm}^{-1}$  above the torsional zero-point energy and the other manifold with eigenvalues grouped octally at about  $89\text{ cm}^{-1}$  above the zero point.

$\text{Ben}(\text{CF}_4)_1$ . Figure 4 and Table II present the  $\text{ben}(\text{CF}_4)_1$  cluster spectrum recorded by 2-color TOFMS in the region between  $38\,578.6$  and  $38\,702.6\text{ cm}^{-1}$ . Unlike the  $\text{ben}(\text{CD}_4)_1$  and  $\text{ben}(\text{CH}_4)_1$  cluster  $6_0^1$  transitions, the  $\text{ben}(\text{CF}_4)_1$  cluster  $6_0^1$  is blue-shifted by  $6.1\text{ cm}^{-1}$  with respect to the benzene  $6_0^1$ . The small hypsochromic shift indicates that the binding energies in the  $S_0$  and  $S_1$  states are nearly identical with ground-state binding energy being slightly greater. The relative displacement between the two potential surfaces is also small since only five vdW transitions are observed, and their intensities decrease abruptly at about  $50\text{ cm}^{-1}$  above the cluster  $6_0^1$  origin. No cluster spectrum is observed in the forbidden benzene  $0_0^0$  region, indicating that the cluster possesses at least a threefold rotation axis. This result is not unexpected since the same observation is made for the  $\text{ben}(\text{CH}_4)_1$  and  $\text{ben}(\text{CD}_4)_1$  systems.

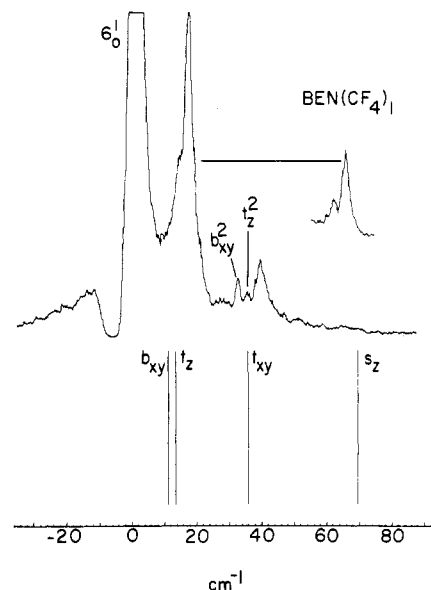


**Figure 4.** Two-color TOFMS  $S_1 \leftarrow S_0$  spectrum and calculated ground-state vdW modes (NCA) of  $\text{ben}(\text{CF}_4)_1$ . Energy scale is relative to  $\text{ben}(\text{CF}_4)_1$   $6_0^1$  transition ( $38\,614.7\text{ cm}^{-1}$ ). Feature positions and assignments as per Table II and Figure 5.

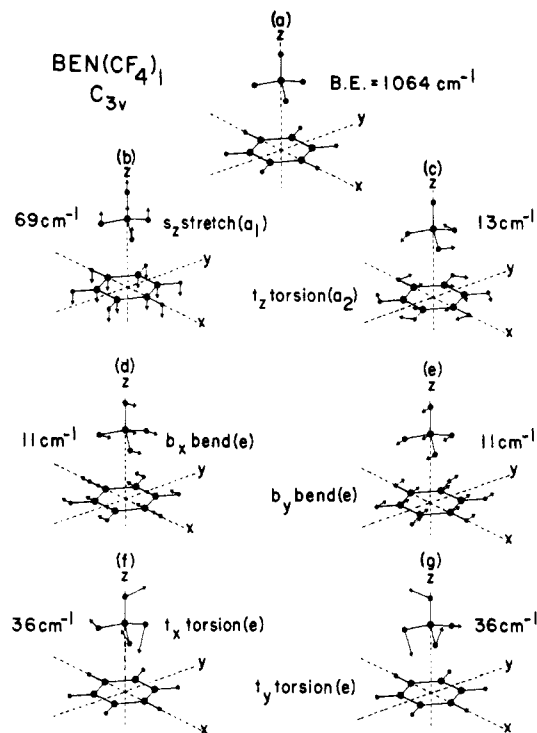


**Figure 5.** Calculated ground-state minimum-energy configuration (a) and NCA eigenvalue/eigenvector normal modes (b)–(g) for  $\text{ben}(\text{CF}_4)_1$ . Cluster symmetry is  $C_{3v}$  with an equilibrium intermolecular distance of  $3.43\text{ \AA}$ . Eigenvectors are normalized and displayed at  $2\times$  magnification ( $2\text{-\AA}$  total displacement).

The ground-state configuration and vdW eigenvalues/eigenvectors are shown in Figure 5 and Table II. Only one minimum-energy geometry is calculated for the cluster. The geometry has  $C_{3v}$  point group symmetry with the  $\text{CF}_4$  center-of-mass at  $3.43\text{ \AA}$  above the benzene molecular plane along the threefold axis. The cluster ground-state binding energy is  $1064\text{ cm}^{-1}$ .

The NCA reveals six vdW vibrations. Their ground-state vibrational energies are  $69\text{ cm}^{-1}$  for the vdW stretch  $s_z(a_1)$ ,  $11\text{ cm}^{-1}$  for the vdW bends  $b_{xy}(e)$ , and  $13\text{ cm}^{-1}$  ( $t_z(a_2)$ ) and  $36\text{ cm}^{-1}$  ( $t_{xy}(e)$ ) for the vdW torsions. The eigenvector normal modes transform as the translational and rotational representations of the  $C_{3v}$  point group as indicated and in the same manner as those for  $\text{ben}(\text{CH}_4)_1$  and  $\text{ben}(\text{CD}_4)_1$ .

## Discussion

In comparing the calculated ground-state vdW vibrational structure and experimental vdW vibronic structure, we assume that the intermolecular potential surfaces of the clusters studied are identical in both the  $S_1$  and  $S_0$  electronic states. Additionally, we utilize the group theoretical arguments developed in our previous publication<sup>3</sup> on vdW cluster vibronic structure to assign and understand the observed cluster spectra.

**Ben(CD<sub>4</sub>)<sub>1</sub>.** The calculated ground-state vdW vibrations (NCA) of ben(CD<sub>4</sub>)<sub>1</sub> and the experimental vibronic spectrum are shown in Figure 2 and Table I. As previously, the assignments are made by direct comparison between the calculations and the experimental vibronic spectra. The intense feature at 22.5 cm<sup>-1</sup> to the blue of the cluster  $6_0^1$  corresponds to the  $t_z$  torsion calculated at 20 cm<sup>-1</sup>. Thus, this feature and its observed overtones at 48.4, 70.5, and 100 cm<sup>-1</sup> are assigned to  $6_0^1$  vdW combination bands  $6_0^1 t_z(a_2)_0^1$ ,  $6_0^1 t_z(a_2)_0^2$ ,  $6_0^1 t_z(a_2)_0^3$ , and  $6_0^1 t_z(a_2)_0^4$ . The features at 32 and 62.7 cm<sup>-1</sup> to the blue of the cluster  $6_0^1$  correspond to the first and third overtones of the twofold degenerate vdW bending modes whose fundamental is calculated at 15 cm<sup>-1</sup>. They are assigned to the  $6_0^1$  combination bands  $6_0^1 b_{xy}(e)_0^1$  and  $6_0^1 b_{xy}(e)_0^2$ , respectively. The feature at 58.1 cm<sup>-1</sup> to the blue of the cluster  $6_0^1$  is assigned to a twofold degenerate  $t_{xy}$  vdW torsions/cluster  $6_0^1$  combination band,  $6_0^1 t_{xy}(e)_0^1$ . The  $t_{xy}$  torsion fundamental is calculated at 64 cm<sup>-1</sup>. With this assignment and that of the  $t_z$  torsion, the feature at 84 cm<sup>-1</sup> is assigned to the  $6_0^1 t_{xy}(e)_0^1 t_z(a_2)_0^1$  combination band. The vdW stretch is calculated at 75 cm<sup>-1</sup>. This mode is identified in the cluster vibronic spectrum at 72.9 cm<sup>-1</sup> to the blue of the cluster  $6_0^1$  origin and is thus assigned as  $6_0^1 s_z(a_1)_0^1$ . Under this scheme, we assign the features at 93.3 and 97.5 cm<sup>-1</sup> as  $6_0^1 s_z(a_1)_0^1 b_{xy}(e)_0^1$  and  $6_0^1 s_z(a_1)_0^1 t_z(a_2)_0^1$  combination bands.

The torsional structure resulting from the 3D-HRRA for ben(CD<sub>4</sub>)<sub>1</sub> (Table I) confirms the torsional assignments made using the NCA. The quartically grouped torsional levels at 21, 46, and 75 cm<sup>-1</sup> correspond to those associated with the  $t_z$  torsion and its overtones in the cluster spectrum at 22.5, 48.4, and 70.5 cm<sup>-1</sup>. The octally grouped torsional levels at 68 cm<sup>-1</sup> correspond to the  $t_{xy}$  torsion assigned at 58.1 cm<sup>-1</sup>.

The correspondence between these levels and those calculated by the NCA can be understood as follows. In the 3D-HRRA, four symmetrically equivalent minima exist in the torsional potential surface. These minima correspond to the four ways of placing the solvent tetrahedron upon the solute with a tetrahedral face toward the solute molecular plane. If the barrier between these minima is infinitely high, penetration of the local wave functions through the barrier separating the potential minima does not take place. In this case, each "well" contains eigenstates corresponding to intermolecular torsions which occur with small amplitude about each potential well minimum. Since the four "potential wells" are identical in shape and depth, a fourfold "structural" degeneracy exists in which all four potential wells contain identical torsional structure. Thus, for example, a non-degenerate torsional eigenstate actually has a fourfold structural degeneracy, etc.

Considering the actual situation in which the potential barrier is finite, tunneling occurs and the "structural" degeneracy is lifted via interaction of the local wave functions through the potential barrier. The eigenstate splitting due to this tunneling may, or may not, be observed depending on the experimental resolution and the relative difference between the eigenstate energy and the barrier height. Splitting of the "structural" degeneracy in the lower portion of the potential well is minimal unless the barrier is low. Based on the calculations, energy level splittings of the first few sets of eigenstates should not be observed unless the barrier is below 150 cm<sup>-1</sup>.

At moderate barriers (about 300 cm<sup>-1</sup>), the eigenstates in the lower portion of the well are nearly degenerate and behave more or less harmonically. For all practical purposes, we can assume these levels to be degenerate. The torsional level structure can then be determined from the eigenstates in one of the minima. Thus, the 3D-HRRA torsional structure calculation simplifies into the NCA. Physically, the cluster can be considered at least

"semirigid" in the respect that it has a definable equilibrium configuration. The potential energy barrier separating one minimum from the others in the potential surface is large and may be of the order of the cluster binding energy.

The vibronic structure in both the ben(CH<sub>4</sub>)<sub>1</sub> and ben(CD<sub>4</sub>)<sub>1</sub> spectra suggests that the systems are more or less rigid. None of the observed vibronic state energies follow a free-rotor formalism for which the energy level structure is described by eq 2. If the systems behaved nonrigidly, the free-rotor eigenstates would lie at approximately  $2.6J(J+1)$  and  $5.2J(J+1)$  cm<sup>-1</sup> for ben(CD<sub>4</sub>)<sub>1</sub> and ben(CH<sub>4</sub>)<sub>1</sub>, respectively, and a  $\Delta J = \pm 1$  selection rule would govern the transitions.

In the ben(CH<sub>4</sub>)<sub>1</sub> and ben(CD<sub>4</sub>)<sub>1</sub> systems, the  $t_z$  torsional mode shifts by 17.6% upon deuterium substitution of the cluster solvent. Both the NCA and 3D-HRRA models predict a 28.6% frequency shift for  $t_z$ , while the free-rotor model would predict a 50% frequency shift for  $t_z$  upon deuteration. Considering that only one mode is taken into account and the mode couplings may be different in the protonated and deuterated clusters, we conclude that torsional tunneling does not take place in the lower levels of the ben(CH<sub>4</sub>)<sub>1</sub> and ben(CD<sub>4</sub>)<sub>1</sub> cluster potential wells and that the clusters can be considered to be rigid.

The negligible isotopic red shift in the  $b_{xy}$  bends also suggest that the cluster is rigid and that the entire observed spectrum is not solely due to internal rotation. The same rationale holds for the vdW stretch: its observation also dispels the notion that only rotor modes occur in the spectrum. No experimental isotopic shift can be determined for the stretching mode, however, since it is not observed in the ben(CH<sub>4</sub>)<sub>1</sub> system. Theoretically, the mode should red shift by 8.5% upon deuteration of the cluster solvent. The ben(CH<sub>4</sub>)<sub>1</sub> stretch should then be at about 80 cm<sup>-1</sup> in the vibronic spectrum based on the observed stretch in the ben(CD<sub>4</sub>)<sub>1</sub> system. (The ben(CH<sub>4</sub>)<sub>1</sub> stretch is calculated by the NCA to be at 82 cm<sup>-1</sup>.)

The ben(CD<sub>4</sub>)<sub>1</sub> cluster spectrum is also substantially richer than the ben(CH<sub>4</sub>)<sub>1</sub> spectrum in the respect that both the vdW stretch and the  $t_{xy}$  torsions are observed along with well-developed  $t_z$  torsion and bend progressions. This is probably due to more favorable Franck-Condon factors in the ben(CD<sub>4</sub>)<sub>1</sub> case resulting from the isotopic substitution.

As is the case for ben(CH<sub>4</sub>)<sub>1</sub>, H-T coupling influences the vibronic intensities (selection rules) in the ben(CD<sub>4</sub>)<sub>1</sub> spectrum. The nontotally symmetric modes  $t_z$ ,  $t_{xy}$ , and  $b_{xy}$  all appear in the spectrum with  $\Delta v = \pm 1, \pm 2, \pm 3, \dots$  selection rules, as can be seen in Figure 2 and Table I.

**Ben(CF<sub>4</sub>)<sub>1</sub>.** Comparison of the calculated ground-state vdW vibrations (NCA) of ben(CF<sub>4</sub>)<sub>1</sub> and the experimental cluster spectrum are presented in Figure 4 and Table II. The intense feature at 17.4 cm<sup>-1</sup> to the blue of the ben(CF<sub>4</sub>)<sub>1</sub>  $6_0^1$  corresponds to the  $t_z$  torsion calculated at 13 cm<sup>-1</sup>. Thus, this feature and its first overtone at 35.4 cm<sup>-1</sup> are assigned to the  $6_0^1$  vdW combination bands  $6_0^1 t_z(a_2)_0^1$  and  $6_0^1 t_z(a_2)_0^2$ . The should feature at 15.7 cm<sup>-1</sup> to the blue of the cluster  $6_0^1$  corresponds to the vdW twofold degenerate  $b_{xy}$  bend fundamental calculated at 11 cm<sup>-1</sup>. Taking this feature as the combination band  $6_0^1 b_{xy}(e)_0^1$  leads to the assignment of the  $b_{xy}$  bend first overtone  $6_0^1 b_{xy}(e)_0^2$  at 32.3 cm<sup>-1</sup>. Finally, the spectral feature at 39.5 cm<sup>-1</sup> in the ben(CF<sub>4</sub>)<sub>1</sub> spectrum corresponds to the  $t_{xy}$  torsion calculated at 36 cm<sup>-1</sup>. Thus, the feature is assigned to the combination band  $6_0^1 t_{xy}(e)_0^1$ .

The ben(CF<sub>4</sub>)<sub>1</sub> spectrum, like the ben(CD<sub>4</sub>)<sub>1</sub> and ben(CH<sub>4</sub>)<sub>1</sub> spectra, suggests that the system is rigid. Since the rotational constant for CF<sub>4</sub> is small (ca. 0.18 cm<sup>-1</sup>), the free-rotor energy level structure should appear at about 0.37-cm<sup>-1</sup> intervals. This structure is not observed. Instead, the spectrum possesses oscillatory torsional structure commensurate with the NCA theoretical predictions. These theoretical and experimental results demonstrate the rigidity of the systems.

The  $S_1 \leftarrow S_0$  excitation of the ben(CF<sub>4</sub>)<sub>1</sub> cluster involves very little change in cluster geometry. In this spectrum, the progression intensities decrease dramatically at energies greater than the  $6_0^1$  cluster origin. In the lowest two vdW mode progressions, the intensities decrease approximately 13% between the mode fun-

damentals and the first overtones. Furthermore, the high-energy vdW stretch calculated at  $69\text{ cm}^{-1}$  is not observed. At these high energies, the Franck-Condon factors must be very small.

The observation of the nontotally symmetric vdW  $b_{xy}$  bends and the  $t_z$  torsion progressions with a  $\Delta v = \pm 1, \pm 2 \dots$  selection rule suggests that interelectronic state mixing (H-T coupling) is an important contributor to the mode intensity mechanism. As in the  $\text{ben}(\text{CH}_4)_1$  and  $\text{ben}(\text{CD}_4)_1$  cases, H-T coupling becomes apparent in the low-lying vdW modes of the  $\text{ben}(\text{CF}_4)_1$  system. In fact, the interelectronic state mixing is substantial in the  $\text{ben}(\text{CF}_4)_1$  system and can be demonstrated by the observation of the well-defined bend fundamental at  $15.7\text{ cm}^{-1}$  and by the observation of the  $t_{xy}$  torsion fundamental ( $39.5\text{ cm}^{-1}$ ). Both of these latter features should not be observed if H-T coupling is not present.

### Summary and Conclusions

Two-color TOFMS and supersonic molecular jet techniques have been employed to study the  $S_1 \leftarrow S_0$  vibronic spectra of  $\text{ben}(\text{CD}_4)_1$  and  $\text{ben}(\text{CF}_4)_1$  vdW clusters. These studies reveal detailed information regarding the geometries, the intermolecular energetics, and the physical nature of the vdW interactions present in the systems. The experimental observations demonstrate that the clusters are at least semirigid systems possessing unique equilibrium geometries and that the intermolecular motion present in the systems is oscillatory. Through comparison of these spectra with those of  $\text{ben}(\text{CH}_4)_1$  previously studied in this laboratory, the "isotopic" shifts observed in the intermolecular vibronic structures demonstrate that all the low-lying intermolecular eigenstates are nearly harmonic. They are not admixtures of oscillatory intermolecular bends and stretches and free intermolecular rotation as would occur if the clusters behaved nonrigidly.

Both the NCA and 3D-HRRA models indicate that the intermolecular torsional motion is oscillatory and that the motion is constrained by an orientationally dependent intermolecular potential. Detailed analysis of the intermolecular interaction reveals that the torsional motion is governed by a three-dimensional potential possessing torsional barriers on the order of the cluster binding energy. At this barrier magnitude, torsional tunneling in the lower portions of the potential is minimal and the residence time of the cluster constituents in a particular well minimum is

substantially longer than the time scale of experimental observation.

The assignment of geometry and identification of the intermolecular modes using the theoretical models has also proven useful in understanding the physics governing the spectroscopic properties of the clusters. The observation of nontotally symmetric intermolecular mode fundamentals and combination bands in the vibronic spectra suggest that interelectronic state mixing (H-T coupling) is an important factor in the overall intensity mechanism governing the transitions. Additionally, the interelectronic state mixing is most important for the low-lying intermolecular bending and torsional modes.

Both the NCA and the 3D-HRRA adequately model the intermolecular modes in the systems studied; however, the NCA is the more useful here due to its mathematical simplicity and passive treatment of all six intermolecular modes in a single calculation. Unlike the 3D-HRRA, the NCA does not require detailed a priori knowledge of the potential surface along each coordinate of motion. Furthermore, the large amount of energy level coupling occurring in the 3D-HRRA at moderate barriers suggests that the model is best used in systems possessing free or nearly free internal rotation.

The rigidity of these clusters can be qualitatively understood by considering the nature of the solvent rotational dynamics. Any rotational state for which  $J \neq 0$  has a displacement in the  $\theta$  coordinate:  $\phi$  and  $\chi$  displacements may or may not be present, depending on the values of the  $k$  and  $m$  quantum numbers. Given the geometry of the system then, low barrier one-dimensional rotation (solvent rotating around the cluster threefold C-X bond axis) is not possible. Basically, the two-dimensional hindering in  $\text{ben}(\text{CX}_4)_1$  clusters is insufficient to produce the one-dimensional rotation occurring in "attached tops" such as toluene.<sup>11</sup>

*Acknowledgment.* We thank Professor W. Klemperer for many helpful discussions and suggestions concerning the rigidity of vdW molecules. This work was supported in part by a grant from ONR.

**Registry No.**  $\text{CD}_4$ , 558-20-3;  $\text{CF}_4$ , 75-73-0; benzene, 71-43-2.

(11) Breen, P. J.; Warren, J. A.; Bernstein, E. R.; Seeman, J. I., to be submitted for publication in *J. Chem. Phys.*

## Studies of Gas-Phase Reactions of Silicon Cation Clusters, $\text{Si}_n^+$ , Using Fourier Transform Mass Spectrometry

William R. Creasy,<sup>†</sup> Anthony O'Keefe,<sup>‡</sup> and J. R. McDonald\*

Chemistry Division, Naval Research Laboratory, Washington, D.C. 20375-5000 (Received: October 31, 1986)

Silicon cation clusters  $\text{Si}_n^+$ ,  $n = 1$  to 6, were formed by laser vaporization of solid silicon with a frequency doubled Nd:YAG laser. The ions were trapped in a Fourier transform mass spectrometer, isolated by mass, and reacted with the neutral gases  $\text{D}_2$ ,  $\text{H}_2\text{O}$ ,  $\text{CH}_3\text{OH}$ ,  $\text{C}_2\text{H}_2$ ,  $\text{NH}_3$ ,  $\text{O}_2$ , and  $\text{N}_2\text{O}$ . Rate constants and product branching ratios are reported for all the reactions. The trends in reactivity as a function of cluster size are discussed in terms of a mechanism and schematic reaction coordinate. The gas-phase reactions are compared to silicon surface reactions.

### Introduction

Ionic and neutral cluster species of silicon<sup>1-15</sup> are interesting from a variety of perspectives. The small clusters have unusual structural, electronic, and chemical properties compared to other molecular ions. With increasing cluster size, the properties of clusters approach those of bulk materials and interfaces. Thus,

the study of cluster properties can give insight into the properties of solids. The study of silicon clusters is particularly relevant to

(1) Honig, R. E. *J. Chem. Phys.* **1954**, *22*, 1610.

(2) Heath, J. R.; Liu, Y.; O'Brien, S. C.; Zhang, Q.-L.; Curl, R. F.; Tittel, F. K.; Smalley, R. E. *J. Chem. Phys.* **1985**, *83*, 5520.

(3) Bloomfield, L. A.; Freeman, R. R.; Brown, W. L. *Phys. Rev. Lett.* **1985**, *54*, 2246.

(4) Furstenuau, N.; Hillenkamp, F. *Int. J. Mass. Spectrom. Ion Phys.* **1981**, *37*, 135.

(5) Martin, T. P.; Schaber, H. Z. *Phys. B* **1979**, *B35*, 61.

<sup>†</sup>NRC/NRL Postdoctoral Research Associate.

<sup>‡</sup>Current address: Western Research Corp., 9555 Distribution Ave., San Diego, CA.